CrystEngComm

ROYAL SOCIETY OF CHEMISTRY

COMMUNICATION

View Article Online
View Journal | View Issue

Check for updates

Cite this: *CrystEngComm*, 2026, **28**, 631

Received 21st November 2025,
Accepted 21st December 2025

DOI: 10.1039/d5ce01108f

rsc.li/crystengcomm

A dynamic pcu MOF(Zn) containing a ditopic T-shaped [2]rotaxane linker

Hazem Amarne,[a] Alexander J. Stirk,[b] Christopher A. O'Keefe,[b] Robert W. Schurko[cd] and Stephen J. Loeb*[b]

A 3D metal–organic framework, designated UWDM-16, formula $[Zn_6(\mu_3\text{-}OH)_2(\mu_2\text{-}RCO_2)_6(\eta^1\text{-}RCO_2)_4(\eta^1\text{-}RCO_2H)_2(H_2O)]$, with a (12)-c hexanuclear SBU was synthesized using a T-shaped [2]rotaxane linker and $Zn(NO_3)_2{\cdot}6H_2O$ under solvothermal conditions in DMF.

Previous efforts to prepare MOFs that incorporate [2]rotaxanes by utilising reticular design strategies[1–12] focused on derived nets containing two geometry dictating branch points with a transitivity, *p q*, of 2 2 (**fof** and **lil** specifically).[13–17] This led to the utilization of diisophthalic and extended diisophthalic linkers that yielded MOF structures related to the well-known **NOTT** series,[18–23] but also some new and quite complex arrangements of linkers and SBUs.[1,24–26] In order to simplify the resulting MOF structures, it was decided to explore edge transitive (*p q* of 1 1) nets[27] that utilise linear linkers without branch points. In particular, the reticular design of Yaghi's iconic **IRMOF** series was targeted for inclusion of a T-shaped, [2]rotaxane linker.[28]

Yaghi and coworker's **IRMOF-15** and **-16** use the linear ditopic linker, 1,1′:4′,1″-terphenyl-4,4″-dicarboxylic acid (**TPDC**), to form **pcu** nets. The former has a two-fold interpenetrated lattice and a void space of 80%, while the latter is not interpenetrated and has a larger void space of 91%.[28] It is our contention that these void spaces, can be utilised as "free volume" to be filled when utilising bulkier linkers. This approach was successful for **IRMOF-77**,[29] which contains the T-shaped ditopic linker [4,7-bis(4-carboxylphenyl)-1,3-dimethylbenzimidazol-2-ylid-ene](pyridyl) palladium(II)iodide (**TPDC-Benz-PdI**), allowing the Pd^{II} moieties to protrude into the available pores of the structure without obvious steric issues.[13,30–34]

Herein, analogous reticular synthesis is applied to T-shaped ditopic linkers and octahedral Zn SBUs to target an edge transitive **pcu** net that allows incorporation of a compact [2]rotaxane. The [2]rotaxane **6** and naked axle analogue **3** used in this study are shown in Fig. 1. Although an edge-transitive pcu MOF, **UWDM-16** (**UWDM** = **U**niversity of **W**indsor **D**ynamic **M**aterial) was formed it contained an unexpected (12)-c hexanuclear SBU, rather than the ubiquitous tetra-zinc oxide cluster of the **IRMOF** series.[35–37]

Scheme 1 outlines the synthetic routes to linkers axle **3** and [2]rotaxane **6**. The benzimidazole group of the linkers was produced from the condensation of 1,2-diamino,3,6-dibromobenzene with 3,5-dimethoxybenzaldehyde. This was followed by a double Suzuki cross-coupling reaction to produce the diester **2**. Upon protonation with HBF_4, the ester $[H\text{-}2]^+$ is capable of acting as a template for the Grubb's G1 catalyzed ring closure of a diolefin polyether to create a [2]

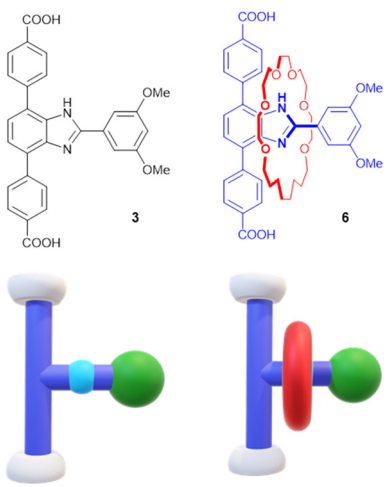

Fig. 1 Linear, ditopic T-shaped linkers; axle (left) and [2]rotaxane (right) linkers **3** and **6** along with their representative carton depictions. Blue = T-shaped benzimidazole unit, red = 24-membered macrocycle (**24C6**), green = 1,3-dimethoxyphenyl stopper, grey = carboxylate groups for coordination to SBUs.

[a] *Department of Chemistry, The University of Jordan, Amman, 11942, Jordan*
[b] *Department of Chemistry and Biochemistry, University of Windsor, Windsor, ON, Canada N9B 3P4. E-mail: loeb@uwindsor.ca*
[c] *Department of Chemistry and Biochemistry, Florida State University, Tallahassee, FL, 32306 USA*
[d] *National High Magnetic Field Laboratory, Tallahassee, FL 32310, USA*

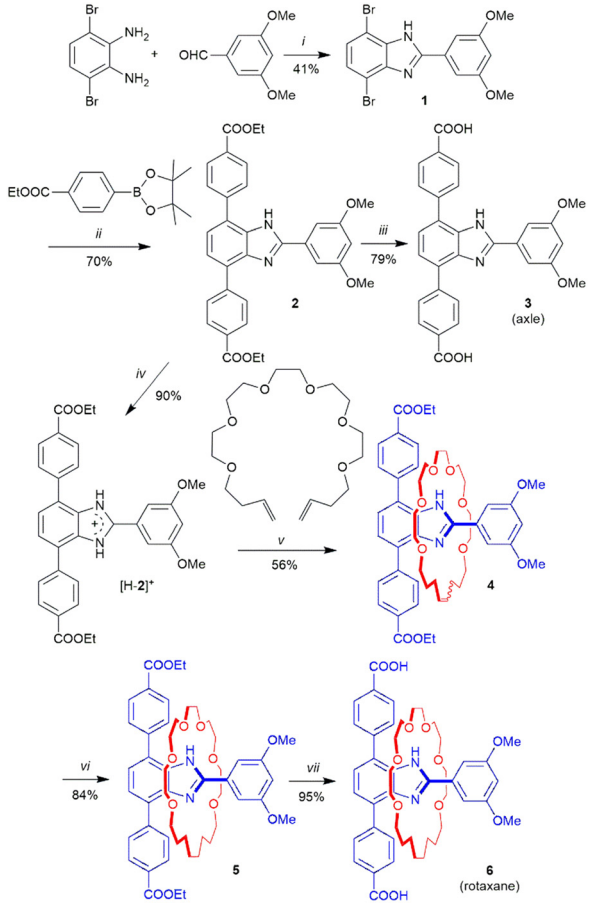

Scheme 1 Synthesis of linkers, axle **3** and [2]rotaxane **6**. i) $ZrCl_4$, O_2, CH_2Cl_2/CH_3CN, RT, 12 h; ii) $[Pd(PPh_3)_4]$ cat., K_2CO_3, THF/H_2O (1 : 1), N_2, 75 °C, 24 h; iii) NaOH, THF/EtOH (1 : 1), 80 °C, 12 h; iv) $HBF_4{\cdot}Et_2O$, Et_2O; v) Grubb's cat. (Gen-1), CH_2Cl_2, N_2, 40 °C, 3d; vi) D_2(g), Pd/C, (10%), MeOH, RT, 6 h; vii) NaOH, THF/EtOH (1 : 1), 80 °C, 12 h.

rotaxane **4**. Reduction of this olefinic precursor using H_2 (or D_2) over Pd/C yielded the diester **5**. Diesters **2** and **5** were then hydrolyzed in basic solution to yield the diacid linkers **3** and **6** respectively. Full characterization (^{1}H and ^{13}C NMR, ESI-MS) of **3** and **6** are described in the ESI, including the SCXRD structure of the diester rotaxane **5** which clearly shows the mechanically interlocked nature of the product (see SI Fig. S4).

UWDM-16 were prepared *via* a solvothermal reaction at 85 °C using $Zn(NO_3)_2{\cdot}6H_2O$ and linker **6** in DMF/EtOH/H_2O in a 3 : 2 : 2 v/v ratio. Large, colourless rhomboid crystals were isolated after 12 h. Attempts to grow single crystals of analogous **UWCM-16** (**UWCM** = **U**niversity of **W**indsor **C**rystalline **M**aterial) employing linker **3** under the same solvothermal conditions resulted only in the isolation of a white powder. PXRD data for activated **UWCM-16** indicated that this is a robust material, perhaps similar to **UWDM-16**, but no conclusion as to the exact nature of the structure was possible. Although several MOF models were investigated based on related penetrated and non-penetrated **IRMOF**s, no match between simulated and experimental PXRD could be achieved (see SI Fig. S8).

Crystals obtained directly from the synthesis of **UWDM-16** were suitable for SCXRD. The structure was shown to have formula $[Zn_6(\mu_3\text{-}OH)_2(\mu_2\text{-}RCO_2)_6(\eta^1\text{-}RCO_2)_4(\eta^1\text{-}RCO_2H)_2(H_2O)]$ and crystallized in the space group $R\bar{3}$.Each face of the created cubes are filled with the [2]rotaxane such that each pore contains two [2]rotaxanes facing each other (Fig. 2).

The SBU created during synthesis was different from the standard octahedral cluster (6)-c $[Zn_4(\mu_4\text{-}O)(\mu_2\text{-}O_2CR)_6]$ usually observed in IRMOFs. Instead, a (12)-c cluster with the overall formula $[Zn_6(\mu_3\text{-}OH)_2(\mu_2\text{-}RCO_2)_6(\eta^1\text{-}RCO_2)_2(\eta^1\text{-}RCO_2H)_4(\mu\text{-}H_2O)]$ was observed (Fig. 3).

Six of the carboxylate groups form expected interactions with Zn, μ_2-bridging pairs of Zn atoms to form distorted tetrahedrons containing apical μ_3-hydroxides. The other six carboxylates interact with Zn ions through a single C–O–Zn bond and four of these carboxylates remain protonated. A single H_2O molecule occupies the centre of the cluster hydrogen bonding to both HOOCR and hydroxide groups. This hexanuclear cluster has not previously been reported, though the bonding arrangement of the Zn(II) ions is quite similar to the heptanuclear, bimetallic (12)-c cluster, $[NaZn_6(\mu_3\text{-}OH)_2(O_2C\text{–})_{12}]$, reported by Ng and coworkers.[38] (see SI Fig. S7).

The reason for formation of this unique cluster may be due to the purposeful presence of H_2O during the synthesis. As a general rule, Zn containing MOFs avoid the use of excess H_2O during synthesis; however, multiple attempts at forming a Zn MOF with **6** under anhydrous conditions produced only amorphous or semi-crystalline material that could not be characterised by X-ray diffraction. However, the addition of a small amount of water produced large single crystals, so it is

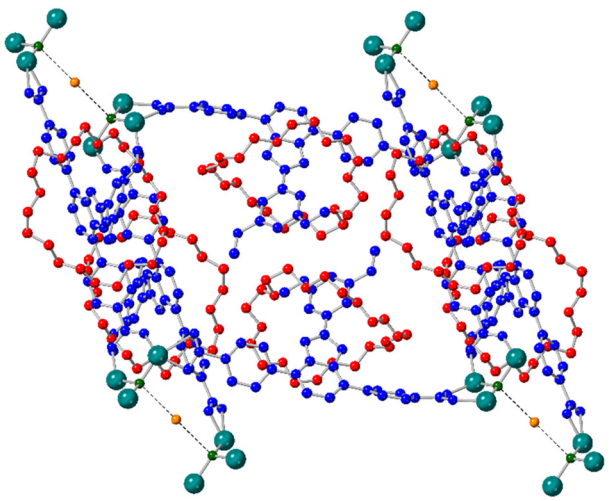

Fig. 2 Single crystal X-ray structure of **UWDM-16** showing connectivity between [2]rotaxane linkers and Zn(II) ions and emphasizing the orientation and approach of two [2]rotaxanes linkers within the pore. T-shaped dicarboxylate axle = blue, crown ether wheel = red, Zn(II) ions = teal, μ_3-OH = green, water = orange. H-atoms are omitted for clarity.

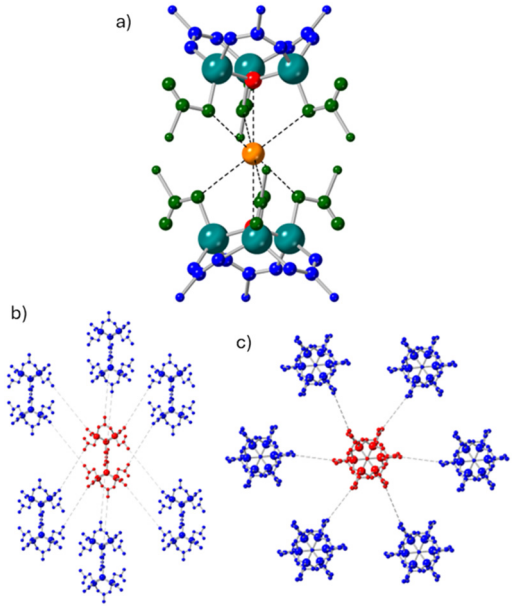

Fig. 3 Single crystal X-ray structure of **UWDM-16**. (a), a Zn cluster showing six Zn(II) atoms (teal), two μ_3-OH groups (red), six μ_2-RCO_2 linkers (blue), six η^1-RCO_2 linkers (green) and a central H_2O molecule (orange). (b) *x*-axis and (c) *z*-axis showing a central cluster (red) with 12 connections to 6 adjacent clusters (blue).

reasonable to surmise that water plays a favourable part in the self-healing process required for MOF synthesis.[39]

It should be noted that since the central water molecule of the SBU only participates *via* non-covalent interactions, **UWDM-16** can be reduced to a $(4^{12}{\cdot}6^3)$ uninodal edge-transitive (6)-c **pcu** net[14,40,41] with a two-fold interpenetration (MOFkey: Zn.JJRWMIIYYSPHFA.MOFkey-v1.pcu).[42]

Most importantly, it is clear that the embedded [2]rotaxane has enough room to fit within the pores created by the framework. ^{2}H VT-SSNMR verified that this positioning of the [2]rotaxane linkers allows for dynamic motion of the macrocycle inside the MOF (Fig. 4).

Conclusions

A T-shaped ditopic linker is a simple and useful design for creating MOFs with mechanically interlocked components and the resulting **pcu** framework allows the interlocked macrocycle to undergo dynamic motion in the solid-state. In the case of **UWDM-16**, reticular synthesis produced a somewhat unique SBU, but this did not fundamentally change the topological connectivity or the transitivity of the linker and still resulted in the targeted **pcu** net. As evidenced by VT-PXRD, this does not appear to greatly affect the thermal stability of the MOF. Further studies are needed to ascertain the overall chemical stability and reactivity of MOFs with this new SBU and elucidate the exact structure of **UWCM-16**.

Author contributions

Conceptualization, S. J. L. and A. J. S.; synthesis, H. A. and A. J. S.; materials characterisation, H. A. and A. J. S.; investigation – SCXRD; A. J. S. and S. J. L. SSNMR; C. A. O.; formal analysis – SSNMR, C. A. O. and R. W. S.; writing – original draft, A. J. S.; writing – review & editing, S. J. L., H. A. and A. J. S.; funding acquisition, S. J. L. and R. W. S.

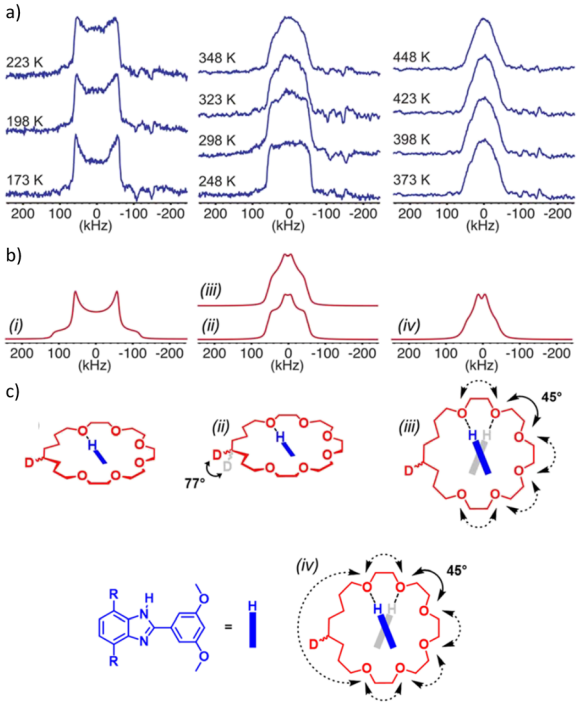

Fig. 4 a) Experimental VT ^{2}H SSNMR powder patterns for **UWDM-16**. b) Simulated ^{2}H SSNMR powder patterns for (i) motions too slow to influence the appearance of the Pake doublet, (ii) a two-site jump motion in the fast motion limit (FML, $\nu_{ex} > 10^6$ Hz) (iii) FML two-site jumps and 1 kHz partial rotation of the ring over 225° in 45° steps, and (iv) FML two-site jumps and 20 kHz partial rotation. c) Four possible modes of rotation around the benzimidazole axle. (i) Immobile (173–223 K). (ii) Two-site jump in the FML (248–348 K). (iii) Partial rotation (373–448 K). (iv) Full rotation including jumps over the full length of the alkyl chain (not observed in **UWDM-16**).

Conflicts of interest

There are no conflicts to declare.

Data availability

The synthetic protocols, NMR and MS data supporting this article have been included as part of the supplementary information (SI).

Supplementary information: synthetic details, ^{1}H, ^{13}C NMR spectra and MS data for all new compounds; PXRD data for **UWCM16** and **UWDM-16**. See DOI: https://doi.org/10.1039/d5ce01108f.

CCDC 2500692 (2), 2500693 (5) and 2500694 (**UWDM-16**) contain the supplementary crystallographic data for this paper.[43a–c]

References

1 B. H. Wilson and S. J. Loeb, in *Mechanically Interlocked Materials*, 2024, pp. 147–176.
2 P. Martinez-Bulit, A. J. Stirk and S. J. Loeb, *Trends in Chemistry*, 2019, **1**, 588–600.
3 N. Farahani, K. Zhu, C. A. O'Keefe, R. W. Schurko and S. J. Loeb, *ChemPlusChem*, 2016, **81**, 836–841.
4 P. Martinez-Bulit, C. A. O'Keefe, K. Zhu, R. W. Schurko and S. J. Loeb, *Cryst. Growth Des.*, 2019, **19**, 5679–5685.
5 D. J. Mercer, J. Yacoub, K. Zhu, S. K. Loeb and S. J. Loeb, *Org. Biomol. Chem.*, 2012, **10**, 6094–6104.
6 V. N. Vukotic, K. J. Harris, K. Zhu, R. W. Schurko and S. J. Loeb, *Nat. Chem.*, 2012, **4**, 456–460.
7 V. N. Vukotic and S. J. Loeb, *Chem. Soc. Rev.*, 2012, **41**, 5896–5906.
8 V. N. Vukotic, C. A. O'Keefe, K. Zhu, K. J. Harris, C. To, R. W. Schurko and S. J. Loeb, *J. Am. Chem. Soc.*, 2015, **137**, 9643–9651.
9 K. Zhu, C. A. O'keefe, V. N. Vukotic, R. W. Schurko and S. J. Loeb, *Nat. Chem.*, 2015, **7**, 514–519.
10 K. Zhu, V. N. Vukotic, C. A. O'Keefe, R. W. Schurko and S. J. Loeb, *J. Am. Chem. Soc.*, 2014, **136**, 7403–7409.
11 P. R. McGonigal, P. Deria, I. Hod, P. Z. Moghadam, A.-J. Avestro, N. E. Horwitz, I. C. Gibbs-Hall, A. K. Blackburn, D. Chen and Y. Y. Botros, *Proc. Natl. Acad. Sci. U. S. A.*, 2015, **112**, 11161–11168.
12 G. Gholami, B. H. Wilson, K. Zhu, C. A. O'Keefe, R. W. Schurko and S. J. Loeb, *Faraday Discuss.*, 2021, **225**, 358–370.
13 A. J. Stirk, B. H. Wilson, C. A. O'Keefe, H. Amarne, K. Zhu, R. W. Schurko and S. J. Loeb, *Nano Res.*, 2021, **14**, 417–422.
14 M. Li, D. Li, M. O'Keeffe and O. M. Yaghi, *Chem. Rev.*, 2014, **114**, 1343–1370.
15 Y. Zhou and L. Han, *Coord. Chem. Rev.*, 2021, **430**, 213665.
16 J. A. Perman, A. J. Cairns, Ł. Wojtas, M. Eddaoudi and M. J. Zaworotko, *CrystEngComm*, 2011, **13**, 3130–3133.
17 H.-L. Xu, X.-S. Zeng, J. Li, Y.-C. Xu, H.-J. Qiu and D.-R. Xiao, *CrystEngComm*, 2018, **20**, 2430–2439.
18 X. Lin, I. Telepeni, A. J. Blake, A. Dailly, C. M. Brown, J. M. Simmons, M. Zoppi, G. S. Walker, K. M. Thomas and T. J. Mays, *J. Am. Chem. Soc.*, 2009, **131**, 2159–2171.
19 J. Jiao, H. Liu, D. Bai and Y. He, *Inorg. Chem.*, 2016, **55**, 3974–3979.
20 Z. Fan, J. Wang, W. Wang, S. Burger, Z. Wang, Y. Wang, C. Wöll, M. Cokoja and R. A. Fischer, *ACS Appl. Mater. Interfaces*, 2020, **12**, 37993–38002.
21 J. J. Perry IV, S. L. Teich-McGoldrick, S. T. Meek, J. A. Greathouse, M. Haranczyk and M. D. Allendorf, *J. Phys. Chem. C*, 2014, **118**, 11685–11698.
22 V. B. López-Cervantes, J. L. Obeso, A. Yañez-Aulestia, A. Islas-Jácome, C. Leyva, E. González-Zamora, E. Sánchez-González and I. A. Ibarra, *Chem. Commun.*, 2023, **59**, 10343–10359.
23 I. A. Ibarra, S. Yang, X. Lin, A. J. Blake, P. J. Rizkallah, H. Nowell, D. R. Allan, N. R. Champness, P. Hubberstey and M. Schröder, *Chem. Commun.*, 2011, **47**, 8304–8306.
24 H.-M. Wen, H. Wang, B. Li, Y. Cui, H. Wang, G. Qian and B. Chen, *Inorg. Chem.*, 2016, **55**, 7214–7218.
25 J. Liu, B. Lukose, O. Shekhah, H. K. Arslan, P. Weidler, H. Gliemann, S. Bräse, S. Grosjean, A. Godt and X. Feng, *Sci. Rep.*, 2012, **2**, 921.
26 X. Lin, J. Jia, X. Zhao, K. M. Thomas, A. J. Blake, G. S. Walker, N. R. Champness, P. Hubberstey and M. Schroder, *Angew. Chem., Int. Ed.*, 2006, **45**, 7358.
27 O. Delgado-Friedrichs, M. O'Keeffe and O. M. Yaghi, *Phys. Chem. Chem. Phys.*, 2007, **9**, 1035–1043.
28 M. Eddaoudi, J. Kim, N. Rosi, D. Vodak, J. Wachter, M. O'Keeffe and O. M. Yaghi, *Science*, 2002, **295**, 469–472.
29 K. Oisaki, Q. Li, H. Furukawa, A. U. Czaja and O. M. Yaghi, *J. Am. Chem. Soc.*, 2010, **132**, 9262–9264.
30 X. Li, J. Xie, Z. Du, L. Jiang, G. Li, S. Ling and K. Zhu, *Chem. Sci.*, 2022, **13**, 6291–6296.
31 S. Millan, B. Gil-Hernández, E. Milles, S. Gökpinar, G. Makhloufi, A. Schmitz, C. Schlüsener and C. Janiak, *Dalton Trans.*, 2019, **48**, 8057–8067.
32 X. Jing, H. Meng, G. Li, Y. Yu, Q. Huo, M. Eddaoudi and Y. Liu, *Cryst. Growth Des.*, 2010, **10**, 3489–3495.
33 T. He, Y.-Z. Zhang, X.-J. Kong, J. Yu, X.-L. Lv, Y. Wu, Z.-J. Guo and J.-R. Li, *ACS Appl. Mater. Interfaces*, 2018, **10**, 16650–16659.
34 B. Li, W. Jiang, Y. Xu, Z. Xu, Q. Yan and G. Yong, *Dyes Pigm.*, 2020, **174**, 108017.
35 H. Li, M. Eddaoudi, M. O'Keeffe and O. M. Yaghi, *Nature*, 1999, **402**, 276–279.
36 J. L. Rowsell and O. M. Yaghi, *J. Am. Chem. Soc.*, 2006, **128**, 1304–1315.
37 J. Yang, A. Grzech, F. M. Mulder and T. J. Dingemans, *Microporous Mesoporous Mater.*, 2013, **171**, 65–71.
38 L. Hou, J. P. Zhang, X. M. Chen and S. W. Ng, *Chem. Commun.*, 2008, 4019–4021.
39 E. K. Berdichevsky, V. A. Downing, R. W. Hooper, N. W. Butt, D. T. McGrath, L. J. Donnelly, V. K. Michaelis and M. J. Katz, *Inorg. Chem.*, 2022, **61**, 7970–7979.
40 M. O'Keeffe, M. A. Peskov, S. J. Ramsden and O. M. Yaghi, *Acc. Chem. Res.*, 2008, **41**, 1782–1789.
41 V. A. Blatov and D. M. Proserpio, in *Modern Methods of Crystal Structure Prediction*, Wiley Online Library, 2010, pp. 1–28.
42 B. J. Bucior, A. S. Rosen, M. Haranczyk, Z. Yao, M. E. Ziebel, O. K. Farha, J. T. Hupp, J. I. Siepmann, A. Aspuru-Guzik and R. Q. Snurr, *Cryst. Growth Des.*, 2019, **19**, 6682–6697.
43 (*a*) CCDC 2500692: Experimental Crystal Structure Determination, 2025, DOI: 10.2550/fix.icsd.cc2py5hb; (*b*) CCDC 2500693: Experimental Crystal Structure Determination, 2025, DOI: 10.2550/fix.icsd.cc2py5jc; (*c*) CCDC 2500694: Experimental Crystal Structure Determination, 2025, DOI: 10.2550/fix.icsd.cc2py5kd.